

Flavor Decomposition of Nucleon Structure at a Neutrino Factory

Richard D. Ball¹

*Department of Physics and Astronomy, University of Edinburgh,
Mayfield Road, Edinburgh EH9 3JZ, Scotland*

Deborah A. Harris

Fermi National Accelerator Laboratory, Batavia, Illinois 60510, USA

Kevin S. McFarland

*Department of Physics and Astronomy, University of Rochester,
Rochester, New York 14627, USA*

Abstract

We explore the possibilities for measuring the quark content of the proton and neutron using neutrino beams produced at a muon storage ring. Because of the nature of the beams, small nuclear targets such as hydrogen and deuterium can be considered, as well as polarized targets. The statistics expected from these targets are calculated using nominal muon storage ring intensities, and the resulting statistical errors on the numerous structure functions available are given, for both polarized and unpolarized targets. It is shown that with a relatively small target, the structure functions F_2 , xF_3 , xg_1 and xg_5 for neutrinos and antineutrinos on protons and deuterium, either unpolarized or polarized, could be determined with excellent precision over most of the accessible kinematic range.

1 Introduction

Deep Inelastic Scattering (DIS) has long been the definitive process for the determination of the quark content of protons and neutrons. Charged lepton scattering has dominated the field in terms of precision determinations of the sum of the quark and antiquark distributions, and the associated gluon

¹ Royal Society University Research Fellow

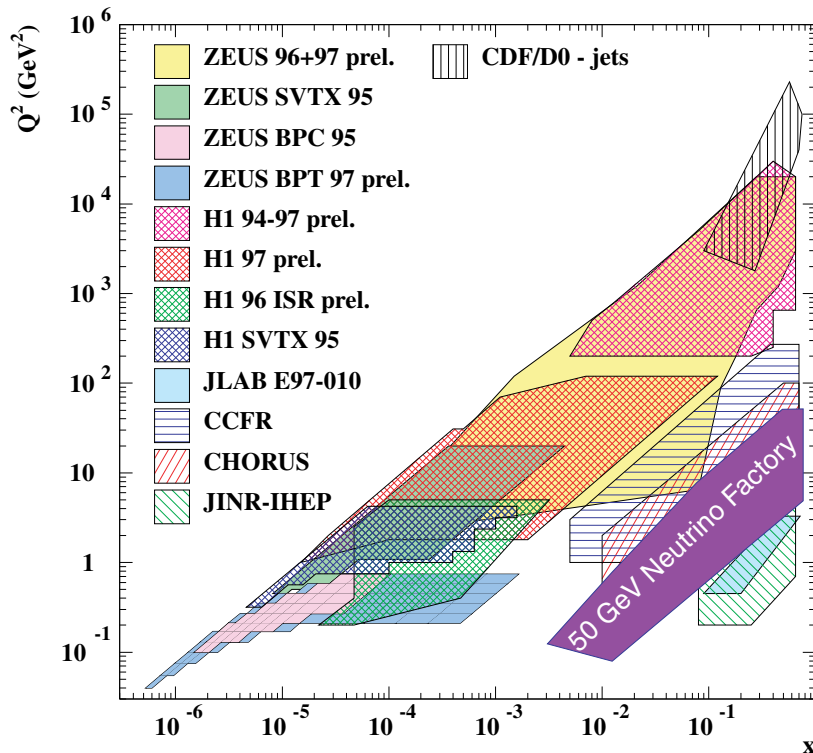


Fig. 1. The kinematic region in the (x, Q^2) plane available at a 50 GeV neutrino factory.

distribution, but neutrino scattering has thus far contributed complementary measurements of the valence quark distributions, as well as measurements of the strange sea. However, neutrino scattering has in the past been plagued by tiny interaction rates and large beam spot sizes, requiring targets on the order of several meters wide and several hundred tons to get appreciable statistics.

With the advent of a muon storage ring the flux of neutrinos at a near detector would be several orders of magnitude higher than at present experiments, and concentrated in a much smaller spot size. Because of this one can now consider using compact hydrogen and deuterium targets, rather than iron. These targets have the advantage of allowing measurements of the valence quark distributions without nuclear effects, or conversely one can finally measure nuclear effects in valence quark distributions by comparing results using different targets. Many of these ideas (as well as other high-rate neutrino experiments at muon storage rings) are considered in references [3],[4], and [5]. Because it is expected that the storage ring will run in roughly equal running times in μ^+ and μ^- mode, the fluxes for ν_e and $\bar{\nu}_e$ will be approximately equal, as will the fluxes for $\bar{\nu}_\mu$ and ν_μ . In conventional beam neutrino experiments the dominant statistical error has been the antineutrino event rate, because the typical total antineutrino event rate (on the targets used) has been only 20-25% of the neutrino event rate.

Aside from just statistical considerations, the neutrino beams from a muon storage ring offer ways to lower previously important systematic uncertainties as well. Because of the well-known incoming ν spectrum one has an accurate determination of the beam energy, as well as a calibration tool for the detector. One also has an extremely pure neutrino beam in terms of sign selection; if μ^- (μ^+) are circulating in the ring the fluxes available are ν_μ and $\bar{\nu}_e$ ($\bar{\nu}_\mu$ and ν_e). By identifying the flavor of the final state lepton in a charged current interaction one knows if the initial lepton was a neutrino or an antineutrino. Finally, again because of the small beam spot size, polarized ν -DIS experiments could be performed for the first time, allowing a full flavor decomposition of the nucleon spin. Because these measurements would still be inclusive DIS measurements, they would not suffer from the fragmentation uncertainties intrinsic to semi-inclusive measurements such as those made at HERMES.

One disadvantage of the neutrino beams from a muon storage ring is that because the rings are expected to operate at a relatively low beam energy (30 to 50 GeV), a lower and smaller range of momentum transfers will be available. The expected kinematic range for a 50 GeV beam is shown in fig1.

The remainder of this paper consists of a description of the theoretical framework by which the quark structure of the nucleon can be measured, a brief discussion of what the neutrino target and detector would look like, and finally, preliminary leading order estimates of expected uncertainties for a variety of structure functions.

2 Unpolarized Structure Functions

Unpolarized charged current structure functions are defined through the decomposition of unpolarized differential charged current cross-sections into invariant functions of the momentum of the struck quark (x) and the momentum transfer squared of the W boson (Q^2): the standard definitions give

$$\frac{d^2\sigma^{\nu\bar{\nu}}}{dx dy} = \frac{G_F^2 S}{2\pi(1+Q^2/M_V^2)^2} [(1-y)F_2^{\nu,\bar{\nu}} + y^2 x F_1^{\nu,\bar{\nu}} \pm y(1-\frac{y}{2})x F_3^{\nu,\bar{\nu}}], \quad (1)$$

where $S = 2mE$ is the centre-of-mass energy, E is the neutrino beam energy, assumed to be $\gg m$, and the \pm signs refer to the sign of the charged current: W^+ exchange for ν scattering and W^- for $\bar{\nu}$. y is the fractional lepton energy loss, or $(E_\nu - E_\ell)/E_\nu$. In neutrino scattering, x , y , and Q^2 can all be determined simply by measuring the outgoing lepton energy and direction, and the hadronic energy in the event. There are then in principle six independent structure functions to be measured for every target. The proton structure

functions are the same as those measured at higher Q^2 (see fig.1 in charged current $e^\pm p$ scattering at HERA).

In the parton model four of these structure functions are related through the Callan-Gross relations $F_2 = 2xF_1$: the longitudinal structure function $F_L = F_2 - 2xF_1$ begins at $O(\alpha_s)$ in perturbation theory. The six structure functions $F_1^{\nu,\bar{\nu}}$, $F_2^{\nu,\bar{\nu}}$ and $F_3^{\nu,\bar{\nu}}$ may in the parton model be expressed in terms of parton densities as

$$\begin{aligned} F_1^\nu &= \bar{u} + d + s + \bar{c}, & F_1^{\bar{\nu}} &= u + \bar{d} + \bar{s} + c, \\ F_2^\nu &= 2x(\bar{u} + d + s + \bar{c}), & F_2^{\bar{\nu}} &= 2x(u + \bar{d} + \bar{s} + c), \\ xF_3^\nu &= 2x(-\bar{u} + d + s - \bar{c}), & xF_3^{\bar{\nu}} &= 2x(u - \bar{d} - \bar{s} + c), \end{aligned} \quad (2)$$

where we have set the CKM mixing angles to zero for simplicity, and restricted attention to the first four flavors.² To go from a proton to a neutron target (assuming isospin invariance) we interchange u and d . It is thus not difficult to see that by constructing appropriate linear combinations of all eight independent structure functions (conventionally taken as $(F_2^{\nu,\bar{\nu}})_{p,n}$ and $(xF_3^{\nu,\bar{\nu}})_{p,n}$) obtained by ν and $\bar{\nu}$ scattering on proton and neutron (or deuteron) targets it is possible to separately disentangle $u \pm \bar{u}$, $d \pm \bar{d}$ and $s \pm \bar{s}$ provided only that we can determine $c \pm \bar{c}$, either theoretically, or else empirically by tagging charm in neutral current processes (as is done currently at HERA). More explicitly, assuming isospin invariance between proton and neutron targets we have

$$\begin{aligned} (F_2^{\nu+\bar{\nu}})_p &= (F_2^{\nu+\bar{\nu}})_n = x(u + \bar{u} + d + \bar{d} + s + \bar{s} + c + \bar{c}), \\ (xF_3^{\nu-\bar{\nu}})_p - (xF_3^{\nu-\bar{\nu}})_n &= -2x(u + \bar{u} - (d + \bar{d})), \\ (xF_3^{\nu-\bar{\nu}})_p + (xF_3^{\nu-\bar{\nu}})_n &= -2x(s + \bar{s} - (c + \bar{c})), \\ (xF_3^{\nu+\bar{\nu}})_p &= (xF_3^{\nu+\bar{\nu}})_n = x(u - \bar{u} + d - \bar{d} + s - \bar{s} + c - \bar{c}), \\ (F_2^{\nu-\bar{\nu}})_p - (F_2^{\nu-\bar{\nu}})_n &= -2x(u - \bar{u} - (d - \bar{d})), \\ (F_2^{\nu-\bar{\nu}})_p + (F_2^{\nu-\bar{\nu}})_n &= -2x(s - \bar{s} - (c - \bar{c})), \end{aligned} \quad (3)$$

where $F_i^{\nu\pm\bar{\nu}} \equiv \frac{1}{2}(F_i^\nu \pm F_i^{\bar{\nu}})$. The first and fourth of these equations are the structure functions $F_2^{\nu+\bar{\nu}}$ and $F_3^{\nu+\bar{\nu}}$ normally measured in neutrino scattering (though on heavy targets), while the second and third allow flavour decomposition of the total $q + \bar{q}$ distributions, and the fifth and sixth a similar decomposition for the valence distributions. To separate out strangeness from intrinsic charm empirically would require either a tagging of charm in the final state to give an independent determination of strangeness alone, or (in principle at least) a combined analysis with neutral current structure function data.

² It is inappropriate to consider only three flavors in charge current scattering since scattering off a strange quark produces a charmed quark in the final state.

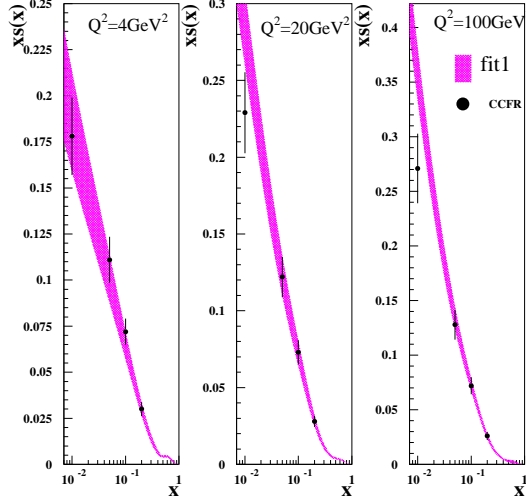


Fig. 2. A strange quark distribution extracted from charged current cross section data [6]: results from a NLO CCFR dimuon determination[7] are shown for comparison.

In perturbative QCD it is possible to perform a complete NLO global analysis using well known results for NLO coefficient functions and anomalous dimensions. The charm contribution can then be computed perturbatively (on the assumption that the intrinsic charm is very small). Since only $F_2^{\nu+\bar{\nu}}$ contains a singlet component, while $F_2^{\nu-\bar{\nu}}$ and $F_3^{\nu\pm\bar{\nu}}$ are entirely nonsinglet, a clean extraction of both α_s [1] and the gluon distribution from scaling violations is possible with data taken over a sufficiently wide kinematic range. To perform such an analysis it is necessary to either extract the structure functions from the differential cross section in a model independent way [2], or simply to fit directly to the cross section [6]. Fits to BEBC,CDHS and CDHSW data suggest that it is already possible to extract $s + \bar{s}$ (see fig. 2) and possibly even $s - \bar{s}$: it will be interesting to see the results of this type of analysis applied to the much more precise CCFR/NuTeV data.

3 Polarized Structure Functions

Polarized structure functions may be defined in analogy with the unpolarized ones through asymmetries in the polarized cross-sections: for longitudinal polarization we may write

$$\frac{d^2 \Delta\sigma^{\nu,\bar{\nu}}}{dx dy} = \frac{G_F^2 S}{2\pi(1+Q^2/M_W^2)^2} \left[\pm y \left(1 - \frac{y}{2} - \frac{xy m}{2E} \right) 2x g_1^{\nu,\bar{\nu}} \mp \frac{2x^2 y m}{E} g_2^{\nu,\bar{\nu}} \right. \\ \left. + \left(1 - y - \frac{xy m}{2E} \right) \left(g_4^{\nu,\bar{\nu}} + \frac{xm}{E} (g_4^{\nu,\bar{\nu}} - g_3^{\nu,\bar{\nu}}) \right) + y^2 x \left(1 + \frac{xm}{E} \right) g_5^{\nu,\bar{\nu}} \right], \quad (4)$$

where the polarization asymmetry $\Delta\sigma = \sigma_{\Rightarrow}^{\leftarrow} - \sigma_{\Leftarrow}^{\leftarrow}$ (the unpolarized cross-section (1) being $\sigma = \frac{1}{2}(\sigma_{\Rightarrow}^{\leftarrow} + \sigma_{\Leftarrow}^{\leftarrow})$), which accounts for the extra factor of 2 on the right hand side of (4)). With these definitions[8]³ in the high energy limit $E \gg m$ g_2 and g_3 drop out, and we are left with an expression of the same form as the unpolarized decomposition (1), but with $F_1 \rightarrow g_5$, $F_2 \rightarrow g_4$ and $F_3 \rightarrow 2g_1$. Thus we again have six partonic structure functions for every target and for high energy polarization asymmetries the complicated decomposition (4) then becomes simply

$$\frac{d^2\Delta\sigma^{\nu,\bar{\nu}}}{dx dy} = \frac{G_F^2 S}{\pi(1+Q^2/M_W^2)^2} [\pm y(1 - \frac{y}{2})2xg_1^{\nu,\bar{\nu}} + (1-y)g_4^{\nu,\bar{\nu}} + y^2xg_5^{\nu,\bar{\nu}}]. \quad (5)$$

The remaining four structure functions $g_2^{\nu,\bar{\nu}}$ and $g_3^{\nu,\bar{\nu}}$ have no simple partonic interpretation and are contaminated by twist three contributions: their twist two components are fixed by the Wandzura-Wilczek relation (giving g_2 in terms of g_1) and a similar relation [8] which gives g_3 in terms of g_4 . They are most easily determined by measuring transverse asymmetries: such measurements are very difficult however because the transverse asymmetry is suppressed by m/Q .

In the parton model g_4 and g_5 are related by an analogue[9] of the Callan-Gross relation: $g_4 = 2xg_5(1+O(\alpha_s))$. The flavor decomposition of the structure functions $g_1^{\nu,\bar{\nu}}$, $g_4^{\nu,\bar{\nu}}$ and $g_5^{\nu,\bar{\nu}}$ may thus be expressed in terms of parton densities as

$$\begin{aligned} g_1^{\nu} &= \Delta\bar{u} + \Delta d + \Delta s + \Delta\bar{c}, & g_1^{\bar{\nu}} &= \Delta u + \Delta\bar{d} + \Delta\bar{s} + \Delta c, \\ g_4^{\nu} &= 2x(-\Delta\bar{u} + \Delta d + \Delta s - \Delta\bar{c}), & g_4^{\bar{\nu}} &= 2x(\Delta u - \Delta\bar{d} - \Delta\bar{s} + \Delta c), \\ g_5^{\nu} &= -\Delta\bar{u} + \Delta d + \Delta s - \Delta\bar{c}, & g_5^{\bar{\nu}} &= \Delta u - \Delta\bar{d} - \Delta\bar{s} + \Delta c, \end{aligned} \quad (6)$$

in precise analogy with the unpolarized case (3): comparing (1) with (5), $F_1 \rightarrow g_5$, $F_2 \rightarrow g_4$, $\frac{1}{2}F_3 \rightarrow g_1$ and $q \rightarrow \Delta q$, $\bar{q} \rightarrow -\Delta\bar{q}$ (changing a quark to an antiquark also flips its helicity). Again, by constructing appropriate linear combinations of all eight independent structure functions (conventionally taken as $(g_1^{\nu,\bar{\nu}})_{p,n}$ and $(g_5^{\nu,\bar{\nu}})_{p,n}$) obtained by longitudinally polarized ν and $\bar{\nu}$ scattering on proton and neutron (or deuteron) targets it is possible to separately disentangle $\Delta u \pm \Delta\bar{u}$, $\Delta d \pm \Delta\bar{d}$ and $(\Delta s \pm \Delta\bar{s})$ just as in eq.(4).

Some combinations of the polarized structure functions are of particular interest. For example, writing $g_i^{\nu\pm\bar{\nu}} \equiv \frac{1}{2}(g_i^{\nu} \pm g_i^{\bar{\nu}})$, the first moment of

$$2(g_1^{\nu+\bar{\nu}})_p = 2(g_1^{\nu+\bar{\nu}})_n = \Delta u + \Delta\bar{u} + \Delta d + \Delta\bar{d} + \Delta s + \Delta\bar{s} + \Delta c + \Delta\bar{c} \quad (7)$$

³ There are many variants in the literature: see [8] for a compilation.

is the axial singlet charge a_0 . This is a much more direct measurement than the traditional one through electron-proton or deuteron DIS since in the latter case one must first subtract the octet charge a_8 which is then only determined indirectly through hyperon decays (see [10] for a recent review). Thus in ν -DIS one would have a direct check on the anomalous suppression of a_0 . Similarly first moments of

$$\begin{aligned} (g_5^{\nu-\bar{\nu}})_p - (g_5^{\nu-\bar{\nu}})_n &= -(\Delta u + \Delta \bar{u} - (\Delta d + \Delta \bar{d})), \\ (g_5^{\nu-\bar{\nu}})_p + (g_5^{\nu-\bar{\nu}})_n &= -(\Delta s + \Delta \bar{s} - (\Delta c + \Delta \bar{c})), \end{aligned} \quad (8)$$

give direct measurements of the axial charge a_3 (again currently only measured indirectly through β -decay) and of the contribution of strange quarks to the nucleon spin, as would the tagging of charm in the final state. Flipping the signs, we can also determine the contribution of valence quarks to the spin, since

$$\begin{aligned} 2(g_5^{\nu+\bar{\nu}})_p &= 2(g_5^{\nu+\bar{\nu}})_n = \Delta u - \Delta \bar{u} + \Delta d - \Delta \bar{d} + \Delta s - \Delta \bar{s} + \Delta c - \Delta \bar{c}, \\ (g_1^{\nu-\bar{\nu}})_p - (g_1^{\nu-\bar{\nu}})_n &= -(\Delta u - \Delta \bar{u} - (\Delta d - \Delta \bar{d})), \\ (g_1^{\nu-\bar{\nu}})_p + (g_1^{\nu-\bar{\nu}})_n &= -(\Delta s - \Delta \bar{s} - (\Delta c - \Delta \bar{c})), \end{aligned} \quad (9)$$

so one could even check for intrinsic strange polarization $\Delta s - \Delta \bar{s}$. None of these valence polarizations can be cleanly measured in current polarization experiments.

In practice this flavor separation would be best performed by a global fit in NLO perturbative QCD: all the NLO anomalous dimensions [11] and coefficient functions [12–14] are known, the latter for heavy quarks, so the polarized charm contribution can be computed perturbatively.

4 Estimates of Neutrino interactions and Event Rates

In order to estimate the precision with which the structure functions above can be measured at a neutrino factory on nuclear targets, a GEANT-based Monte Carlo was used, with hydrogen and deuterium chosen as targets. This simulation used LEPTO and JETSET (versions 6.5.1 and 7.408 respectively) to determine what the struck quark and its fragmentation were for each interaction, and the parton densities used were from CTEQ2MS [15]. The hadron showers were not traced through the detector; because of the low densities of the targets and their sizes it is expected that most of the shower will leave the target and be collected in a low mass particle-tracking system. Therefore, in the results described below there is no smearing from detector resolution.

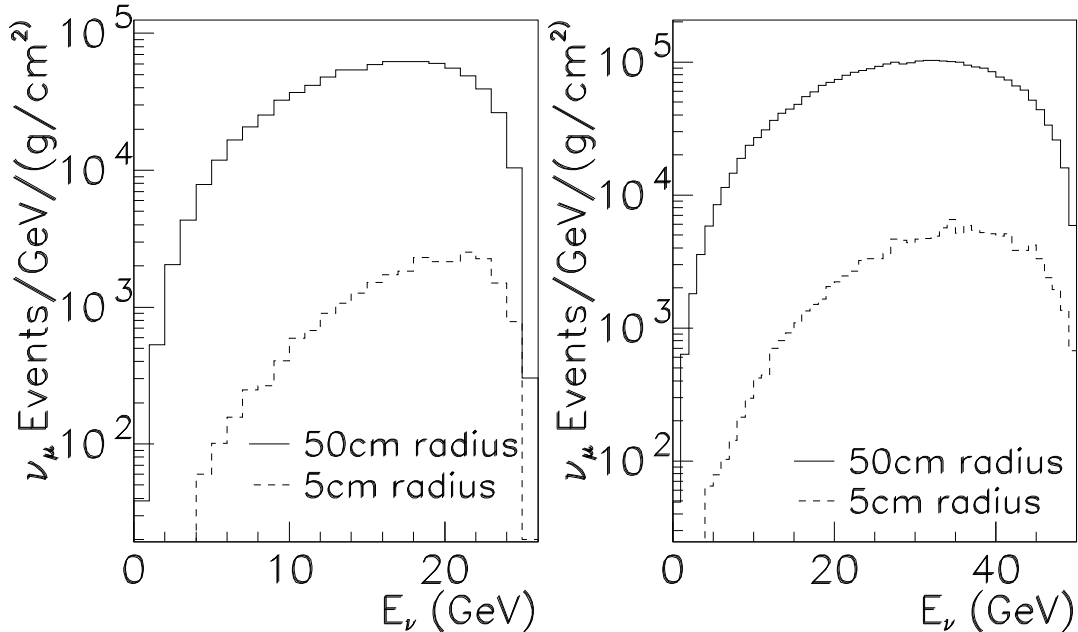


Fig. 3. Number of muon neutrino events per GeV per g/cm^2 for 10^{20} muon decays in an 800m long straight section followed by a 40m shielding section and a detector of radius 5 or 50 cm. Other storage ring parameters are given in the text.

The acceptance for muon neutrino and antineutrino charged current interactions is assumed to be 100% for events with muons above 3 GeV, and to remove events from the quasielastic and resonance region only events with hadron energies above 1 GeV were considered. It should be noted that the precisions listed here are pessimistic, since they are calculated assuming only an incoming $\nu_\mu(\bar{\nu}_\mu)$ flux. The $\bar{\nu}_e(\nu_e)$ fluxes that arrive simultaneously could in principle donate roughly another factor of two in event statistics. However, since the acceptance and backgrounds for ν_e charged current events are much more detector dependent these events are not considered here.

The question of where the high-rate neutrino physics experiments would occur at a neutrino factory is not a trivial one, but for a rough estimate of the overall statistics in neutrino (μ^- in the storage ring) and antineutrino (μ^+ in the storage ring) running, consider two scenarios: a 25 and 50 GeV muon storage ring with 800m straight sections, followed by 30m of active shielding. Two target sizes were considered, namely a 5cm radius or a 50cm radius. In both cases the muon beam spot size was $1.23\text{cm}(x) \times 0.883\text{cm}(y)$, and the muon beam divergence was 0.73 mrad in both the vertical and horizontal directions. Figure 3 shows the muon neutrino fluxes for these different scenarios. The (x, Q^2) regions accessible are comparable between two different radii at the same energy: the most important factor is the loss of statistics for the smaller target. Note that the rate difference between the two radii is roughly 10 at high energies rather than a factor of 100. Table 1 gives the neutrino charged

Muon Energy	Detector Radius	
	5cm	50cm
25 GeV	24.5K	841K
50 GeV	131K	2900K

Table 1

Muon neutrino charged current interaction rates for 10^{20} muon decays (one year) for detectors of different radius and for storage rings of different energies.

current interaction rates for these different scenarios on a 1 g/cm^2 isoscalar target.

Given that the density of cryogenic deuterium is at least 0.162 g/cm^3 , 1 g/cm^2 corresponds to only 6 cm of deuterium. Targets 1.3 meters long of cryogenic (polarized!) material have already been used by SMC, so one can imagine multiplying the statistics listed in table 1 by a factor of 20 and still have a 10 g/cm^2 target after fiducial cuts on the vertex. Much larger targets of liquid Hydrogen have been used in the past in neutrino experiments, but with extremely low neutrino event statistics.

The relative cross sections per nucleon between $\nu D_2 : \bar{\nu} D_2 : \nu H_2 : \bar{\nu} H_2$ are approximately 2:1:1.3:1.3, (as calculated by GEANT) due to the higher abundance of up quarks in H_2 compared to D_2 . For an unpolarized target one can consider radii of 50cm. Due to the strong B field and low temperature requirements for the polarized targets (as well as the small beam spot size), at present only polarized targets of 5cm diameter have been used for charged lepton scattering experiments [16]. Given the rate of advances in cryogenic and magnetic field technology, it is not unreasonable to expect that much larger targets will be available several years from now. For that reason we consider targets of polarized materials that are the same size as the modest unpolarized targets.

5 Unpolarized Cross Sections at a Neutrino Factory

To estimate the uncertainties on the unpolarized structure functions at a muon storage ring experiment, a leading order "model-independent" analysis was performed on the Monte Carlo data, as is described in [2]. Simply put, the differential cross sections are measured in (x, y, E) bins, and then they are collected into (x, y, Q^2) bins, such that for a given (x, Q^2) bin there is a range of neutrino energies contributing as y goes from 0 to 1. The errors on the cross sections in each bin are taken to be the statistical errors alone resulting from the above fluxes (taking into account the total cross section differences between the different targets and probes). For a given (x, Q^2) bin the y distribution is

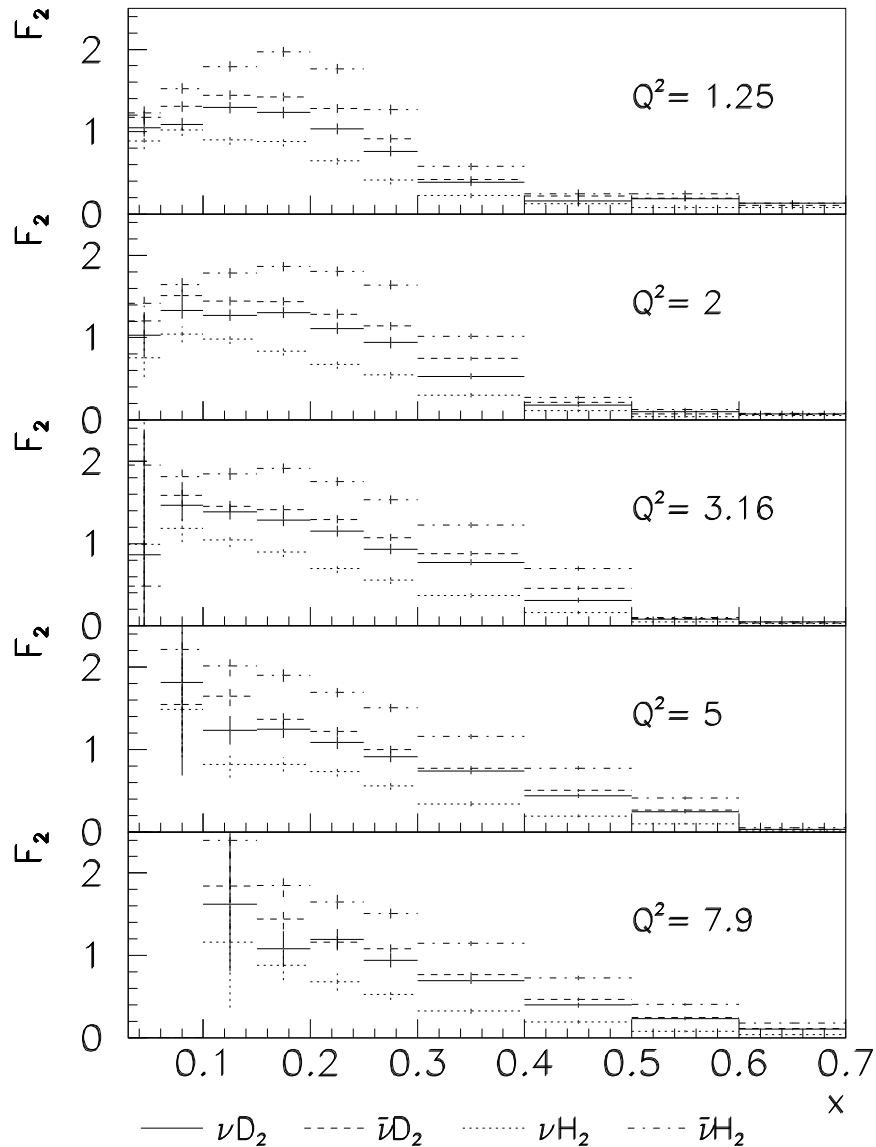


Fig. 4. Expected results for $F_2^{\nu,\bar{\nu}}$ from one year of running in each mode, with a 0.1 g/cm² target: for a 10 g/cm² target the errors would be reduced by a factor of 10.

fit to the function in eqn.(5), setting $2xF_1 = F_2$. This will modify the central values fit since in reality the ratio $R = (F_2 - 2xF_1)/F_2$ is non-zero in neutrino scattering just as it is in electron scattering [17], but the errors on F_2 and xF_3 should not be affected. Also, there are no bin-centering corrections applied here, but the resulting fit errors should again not be affected.

Figures 4 and 5 show the fit results for the structure functions F_2 and xF_3 on both deuterium and hydrogen for both neutrinos and antineutrinos. Because of limited Monte Carlo statistics, the errors shown above are for 0.1 g/cm²

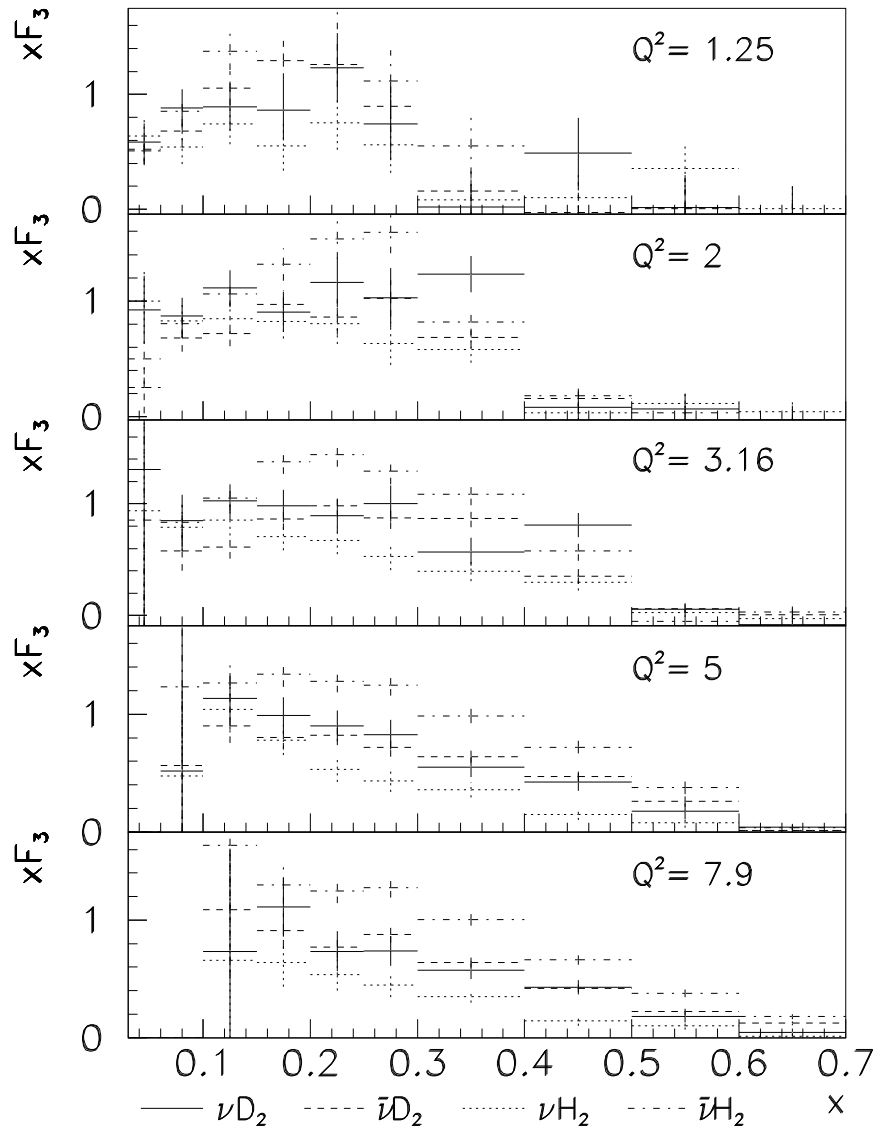


Fig. 5. The same as fig.4, but this time showing results for xF_3 .

targets, for 10^{20} 50 GeV muons decaying in the straight section in each mode (μ^+ and μ^-), and for a target of radius 50 cm. The χ^2 for the fits were roughly at 1 per degree of freedom or better, because the Monte Carlo statistics were slightly higher than the expected experimental statistics for these targets. The error reported by the fit does represent the experimental error expected, however, not the error due to the Monte Carlo statistics.

These data access a Q^2 range that is lower than most of the CCFR data. For the expected precision of a modest-sized target, one would divide these errors by a factor of 10 which assumes a 10 g/cm^2 fiducial target. What makes these

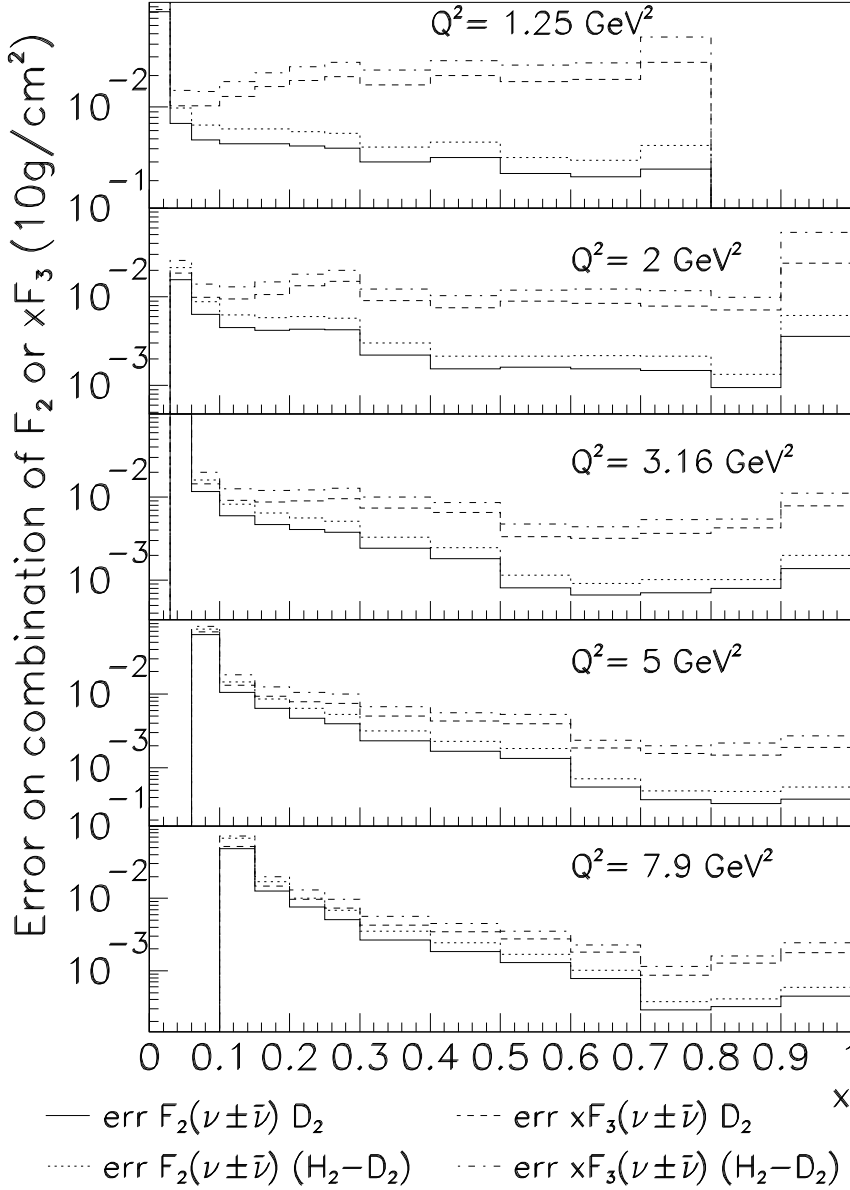


Fig. 6. Estimated errors on $F_2^{\nu\pm\bar{\nu}}$ and $xF_3^{\nu\pm\bar{\nu}}$ after one year of running on each of neutrinos and antineutrinos, on a target of $10g/cm^2$ of D_2 and $H_2 - D_2$ for the range of x and Q^2 space above $Q^2 = 1 \text{ GeV}^2$. Note that one can achieve errors of better than 0.01 on sums and differences of structure functions with these statistics in most of the kinematic range accessed.

measurements unique however is the possibility of taking particular sums and differences between combinations of ν and $\bar{\nu}$, hydrogen and deuterium structure functions. Figure 6 shows the expected errors on the various structure function combinations listed in eqn.4, remembering that $D_2 = \frac{1}{2}(p+n)$, while $(H_2 - D_2) = \frac{1}{2}(p-n)$.

The errors on the sums and differences of F_2 and xF_3 are comparable, but while the sums are of order unity, some of the differences are expected to be quite small. Also, the errors on xF_3 are larger than those for F_2 for every combination, although they approach each other as Q^2 increases. What is important here however is that the errors are uniformly small; less than 0.01 for most of the (x, Q^2) range accessible. For comparison, the statistical errors on $(\nu + \bar{\nu})$ Fe structure functions from CCFR in its kinematic range vary from 0.01 to 0.04 [1].

6 Polarized Cross Sections at a Neutrino Factory

The polarized cross section measurements will be more difficult due to several factors, Firstly, to keep the target polarized it must be in both a strong magnetic field and a very low temperature container, so the target size may be limited to smaller volumes than for unpolarized targets. Secondly, since one is taking differences of cross sections the polarized cross-sections will be smaller than the unpolarized ones and the fractional error correspondingly larger. Finally, the fraction of polarized nuclei will necessarily be lower than 100%. Two possible polarized target materials used in the past in charged lepton scattering are polarized solid butanol (used by the SMC collaboration) [16] or a polarized HD target (used by the LEGS collaboration) [18].

If one only polarizes the hydrogen or the deuterium in the target sample then when one takes the differences between opposite polarizations the result will only depend on the polarized nuclei. In this way one can use deuterated butanol and butanol to measure the D and the H cross section differences. In the HD target, the two components are independently polarizable. So for measurements of p+n or D alone, one can simply polarize the D in the sample and leave the H unpolarized. For measurements of p-n, one can either polarize only the H, or use targets where the the H and the D are polarized in opposite directions. In the latter case one is effectively scattering off polarized neutrons.

To see how the errors on the polarized cross sections compare to those on the unpolarized cross sections, consider the following argument: for a perfectly polarized H_2 target of the same size as that considered above (10g/cm², 50cm radius) if all the protons were polarized, then the error on the cross section difference would roughly be $1/\sqrt{2}$ times the error on the unpolarized case, assuming one integrated 10^{20} muon decays in one polarization and 10^{20} muon decays in the opposite polarization. Factors such as the incomplete polarization of the target and the fact that the polarized target is not 100% H_2 enter into the error in the following way:

Characteristic	p-Butanol	D-butanol	HD(D \uparrow)	HD (H \uparrow D \downarrow)
Density (g/cm^3)	0.61	0.69	0.05	0.05
D/H Polarization	86%	51%	70%	70%(D), 95%(H)
Dilution Factor ν	0.15	0.22	0.4	1.0
Dilution Factor $\bar{\nu}$	0.25	0.22	0.55	1.0
Length (cm)	120	120	10	10
(g/cm^2)	73.2	82.8	0.5	0.5
Diameter (cm)	5	5	3	3
B Field	2.5 T	2.5T	7T	7T
Temperature	0.1K	0.1K	1.5K	1.5K
total target factor (ν)	2.6	4.4	4.3	2.6
total target factor ($\bar{\nu}$)	1.6	4.4	3.1	4.8

Table 2

Comparison of four polarized targets: p-butanol, D-butanol, an HD target with only the D polarized, or HD with both H and D polarized oppositely. The ‘density’ is the effective density for solid butanol (which depends on the packing fraction), and the dilution factors were calculated based on neutrino and antineutrino cross sections on protons and isoscalar nuclei. The total target factor only takes into account the ratio between the given material and liquid H_2 or D_2 densities, the polarization, and the dilution factor.

$$\sigma_{\text{pol}} = \frac{\sigma_{\text{unpol}}}{f_{\nu, \bar{\nu}} P} \sqrt{\frac{\rho_{\text{unpol}}}{\rho_{\text{pol}}}} \quad (10)$$

where $\rho_{\text{unpol}}/\rho_{\text{pol}}$ is the ratio of target densities to H_2 or D_2 , $f_{\nu, \bar{\nu}}$ is the dilution factor and P is the polarization of the H_2 or D_2 . The dilution factor $f_{\nu, \bar{\nu}}$ is the ν (or $\bar{\nu}$) cross-section weighted ratio of the polarized nucleon to total nucleon content of the target. Because the different targets have of necessity different ratios of protons and neutrons, the neutrino and antineutrino dilution factors will be different.

Table 2 compares the SMC and LEGS targets for both the D_2 cross-section difference and the H_2 cross-section difference [16][18][19]. In summary, in the SMC target the density is high but the dilution factor is small, while for the HD target the density is low but the dilution factor is high. The HD target is newer and has not been made in as large samples as the SMC target, but the HD targets are modular and one can easily imagine adding several together. Overall the multiplicative factors coming from target details alone range from 1.6 to 4.8.

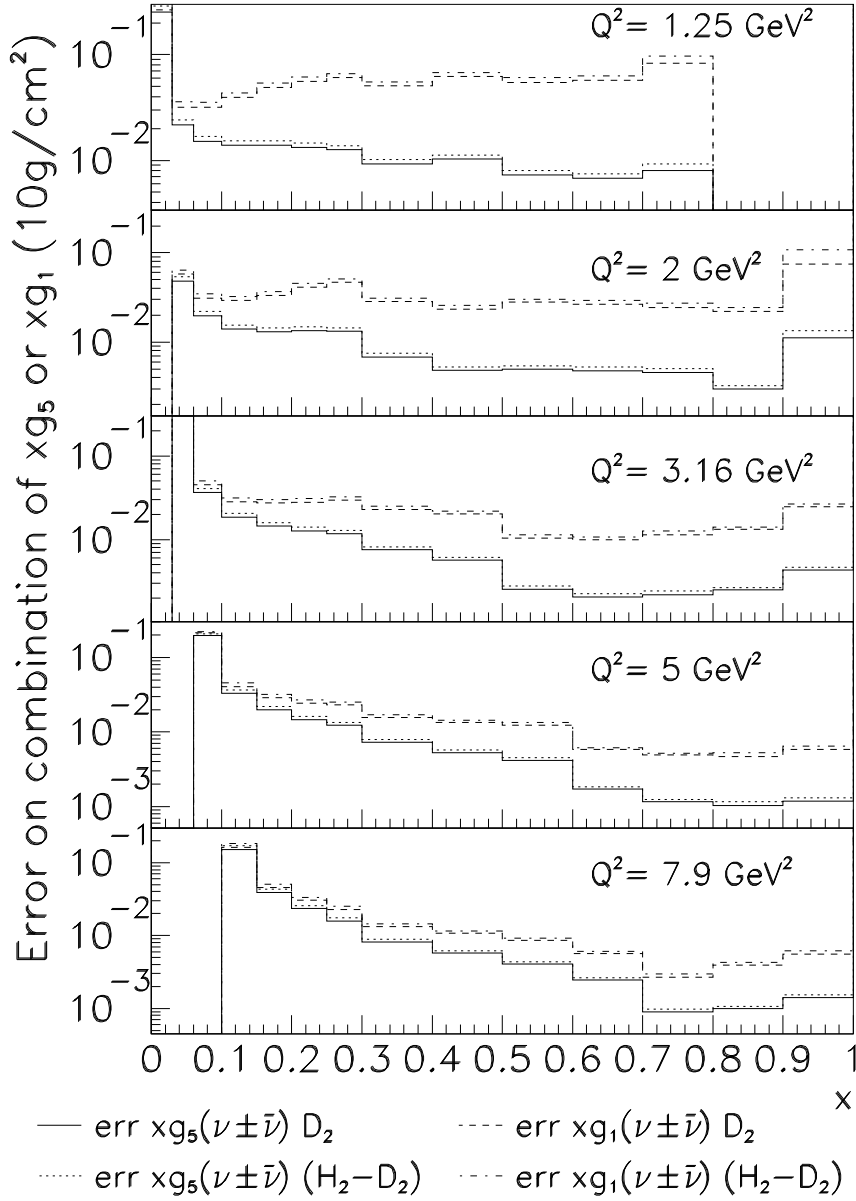


Fig. 7. Error on polarized structure functions on $xg_1^{\nu\pm\bar{\nu}}$ and $xg_5^{\nu\pm\bar{\nu}}$ coming from one year of running for each combination of neutrinos, antineutrinos, polarized solid butanol and deuterated butanol in 2 polarizations for one small range of x and Q^2 space. Note that one can achieve 0.05 errors or better on spin structure functions with these statistics.

To translate between the cross section uncertainty and the polarized structure function uncertainty, recall that the functional form (up to terms in m/E which are going to be small even for a 50 GeV muon storage ring) for the unpolarized cross sections (eqn. 1) is the same as that for the polarized cross sections (eqn. 4), up to the substitutions $F_2 \rightarrow g_4 = 2xg_5$ and $F_3 \rightarrow 2g_1$. Therefore, the error on xg_1 or xg_5 for a given x, Q^2 bin is the same as that of

$x F_3/2$ or $F_2/2$ in the unpolarized case multiplied by the ratio of the errors in the cross sections and the extra $\sqrt{2}$ from having two targets, described above.

Figure 7 shows the resulting errors on the various linear combinations of polarized structure functions, listed in eqn.4, remembering again that $D_2 = \frac{1}{2}(p+n)$, while $H_2 - D_2 = \frac{1}{2}(p - n)$. We have assumed one year's running at each polarization, each neutrino flavor, and each target. Note that at the very least it is assumed that one would run in two target polarizations simultaneously, so this represents a total of 4 to 8 years of running at $10^{20} \mu^\pm$ decays per year. The targets are the same size as in figure 6 but filled with either butanol or deuterated butanol, as was done by SMC [16].

The errors on the sums and differences of xg_1 and xg_5 are comparable, but while the sums are of order unity, some of the differences are again expected to be quite small. Also, the errors on xg_5 are smaller than those for xg_1 for every combination, although they approach each other as Q^2 increases. What is important is that the errors are uniformly small, just as in the unpolarized case: less than a few times 0.01 for most of the accessible (x, Q^2) range.

7 Conclusions

We have examined the novel structure function measurements that could be made at a neutrino factory, and provided estimates of their precision as a function of x and Q^2 for nominal storage ring running (10^{20} muons per year in a 50 GeV muon storage ring). Because of the clean separation between valence and sea afforded by neutrino and antineutrino running and the possibility of using both deuterium and hydrogen targets, such experiments could at last determine flavor by flavor the valence and sea quark distribution functions with statistical errors uniformly of order 0.01 in each bin. Systematic errors due to nuclear effects and beam energy would be minimal. Furthermore, by running with polarized targets already developed by the charged lepton scattering community the spin components of the proton, quark by quark, could be determined for the first time, again with statistical errors uniformly of order a few times 0.01. Such measurements would resolve definitively the questions raised by the EMC experiment, in particular by determining both the strange and gluon contributions simultaneously in one experiment. Combining this data with complementary data from eRHIC or polarized HERA could result in precise tests of our understanding of the spin structure of the nucleon.

A 50 GeV neutrino factory would be an ideal partonometer, revealing the partonic structure of the nucleon in exquisite detail. We hope that it may be possible to enjoy such a facility in the not too distant future.

Acknowledgement:

RDB would like to thank M. Mangano for discussions and correspondence on this subject, and S. Forte for comments on the completed manuscript. DAH would like to thank M. Velasco for discussions and help on this subject, in particular concerning spin physics and novel target techniques. This work was supported in part by EU TMR contract FMRX-CT98-0194 (DG 12 - MIHT).

References

- [1] W.G. Seligman *et al.*, *Phys. Rev. Lett.* **79** (1997) 1213.
- [2] A. Bodek *et al.*, [hep-ex/0005021](#); [hep-ex/0008003](#).
- [3] D.A. Harris, and K.S.McFarland, [hep-ex/9804010](#), proceedings of the Workshop on Physics at the First Muon Collider and at the Front End of a Muon Collider, November 1997, Fermilab.
- [4] I. Bigi *et al.*, The Potential for Neutrino Physics at Muon Colliders and Dedicated High Current Muon Storage Rings, BNL-67404.
- [5] Albright *et al.*, Physics at a Neutrino Factory, FERMILAB-FN-692 [hep-ex/0008064](#).
- [6] V. Barone, C. Pascaud and F. Zomer, *Eur. Phys. J.* **C12** (2000) 243.
- [7] A.O. Bazarko *et al.*, *Zeit. Phys.* **C65** (1989) 189.
- [8] J. Blümlein and N. Kochelev, *Phys. Lett.* **B381** (1996) 296; *Nucl. Phys.* **B498** (1997) 285.
- [9] D.A. Dicus, *Phys. Rev.* **D5** (1972) 1637.
- [10] R.D. Ball and H.A.M. Tallini, *Jour. Phys.* **G25** (1999) 1327, and ref. therein.
- [11] R. Mertig and W. L. van Neerven, *Zeit. Phys.* **C70** (1996) 637; W. Vogelsang, *Phys. Rev.* **D54** (1996) 2023.
- [12] D. de Florian and R. Sassot, *Phys. Rev.* **D51** (1995) 6052.
- [13] M. Stratmann, A. Weber and W. Vogelsang, *Phys. Rev.* **D53** (1996) 138.
- [14] S. Kretzer and M. Stratmann, *Eur. Phys. J.* **C10** (1999) 107.
- [15] J. Botts *et al.*, *Phys. Lett.* **B304** (1993) 159.
- [16] SMC Collaboration CERN-EP/99-31
- [17] U.K.Yang *et al.*, *Nucl. Phys. Proc. Suppl.* **79** (1999) 89.
- [18] A. Honig *et al.*, *Nucl. Inst. Meth.* **A356** (1995) 39.
- [19] The current sizes for the HD targets appearing in the table were given by A. Honig, private communication.
- [20] J. Kyynäräinen, *Nucl. Inst. Meth.* **A356** (1995) 47.